PHOTONICS Research

Grating mediated by three-dimensional director solitons

Chao-Yi Li,[1,2,†] Xing-Zhou Tang,[2,†] Zhi-Jun Huang,[2] Ge Sun,[3] Ze-Yu Wang,[1] Yuan Liu,[1,5] Bing-Xiang Li,[1,2,6] Juan J. de Pablo,[3,4] and Yan-Qing Lu[1,7]

[1]National Laboratory of Solid State Microstructures, College of Engineering and Applied Sciences, and Collaborative Innovation Center of Advanced Microstructures, Nanjing University, Nanjing 210093, China
[2]College of Electronic and Optical Engineering & College of Flexible Electronics (Future Technology), Nanjing University of Posts and Telecommunications, Nanjing 210023, China
[3]Pritzker School of Molecular Engineering, The University of Chicago, Chicago, Illinois 60637, USA
[4]Center for Molecular Engineering, Argonne National Laboratory, Lemont, Illinois 60439, USA
[5]e-mail: liuyuan@nju.edu.cn
[6]e-mail: bxli@njupt.edu.cn
[7]e-mail: yqlu@nju.edu.cn
[†]These authors contributed equally to this work.

Received 6 November 2024; revised 21 April 2025; accepted 20 May 2025; posted 27 May 2025 (Doc. ID 546820); published 28 July 2025

Within the realm of soft matter, particularly liquid crystals, the ability to leverage material properties to create switchable diffraction gratings holds significant importance in disciplines such as optics and information science. However, designing switchable patterns and compiling information based on output images remain challenging. Here, we introduce an approach to address these limitations by designing switchable gratings mediated by three-dimensional director solitons. We utilize photo-patterning, employing lithography systems with different ultraviolet light, to fabricate the desired patterns. This method allows solitons to nucleate and localize within the regions of the pattern where the anchoring energy is weaker. The periodic structures, alternating between solitons and uniform patterns, exhibit the ability to diffract light beams. By switching the voltage, we can control the generation and localization of solitons within periodic patterns and realize switching between the waveplate and grating. Our experimental findings, complemented by simulation outcomes, validate the feasibility of utilizing three-dimensional solitons in optical applications.

https://doi.org/10.1364/PRJ.546820

1. INTRODUCTION

Solitary waves, often termed "solitons", are spatially localized wave packets that propagate at a constant speed while maintaining their shape with minimal dissipation [1,2]. Over the years, solitons have attracted significant interest across various disciplines, including mathematics [3,4], biology [5,6], and physics [7,8], due to their unique properties and potential applications. This interest is inspired by natural phenomena, such as tidal bores, cyclones, and massive ocean waves like tsunamis [9], which serve as real-world examples of soliton behavior.

In orientationally ordered soft matter systems, three-dimensional director solitons resemble bow-shaped distortions of molecular orientation [10–13]. These localized director perturbations can traverse distances several tens of times their own length and survive collisions, showcasing their robustness and persistence [10–12,14,15].

Recently, researchers have developed various mechanisms, such as anchoring [12,16], surface strain [17], ions [18,19], and abrupt changes [12,20–22] in nematic orientations, to achieve kinetic control of director solitons. These advancements have demonstrated that solitons can be employed for micro-cargo transport in both homogeneous systems [11,14] and domains with a gradient of director [21,22] under an applied sinusoidal AC electric field. Given their remarkable properties, a compelling question arises: can director solitons be applied in fields beyond micro-cargo transport?

Liquid crystals (LCs), possessing both fluidity and anisotropies of physical properties, hold significant importance in disciplines such as optics and information science [23–27]. Recently, it has been shown that the Fabry–Perot resonator incorporating a central layer of nematic liquid crystal can serve as a nonlinear polarization rotator for passive Q-switching and mode-locking, with response times on the order of microseconds [28]. Besides, researchers have established grating patterns by periodically aligning the director field of LCs [29–35]. However, these grating patterns were either not erasable or provided limited information in the output images. In this work, we effectively generate and localize three-dimensional director

solitons within orientationally ordered patterns utilizing photoalignment technology. By using a digital micro-mirror device (DMD) micro-lithography system, we precisely orchestrate the size and period of these patterns. The periodic patterns filled with solitons can be regarded as binary amplitude gratings, and their behavior under different electric fields offers varying output images. Our experimental findings, complemented by simulation outcomes, validate the feasibility of utilizing solitons in optical applications. This research not only represents a breakthrough in the design and control of diffraction gratings but also expands the potential applications of LC solitons in information science. By leveraging the unique properties of solitons, we open new avenues for innovative optical devices and advanced information processing techniques.

2. RESULTS AND DISCUSSION

A. Principle of the Grating Mediated by Solitons

A single-component LC, 4′-butyl-4-heptyl-bicyclo-hexyl-4-carbonitrile (CCN-47), with negative dielectric and conductive anisotropies [10] ($\Delta\varepsilon \sim -4.2$, $\Delta\sigma \sim -1.2 \times 10^{-9}\ \Omega^{-1}\ m^{-1}$, at 45°C and 4 kHz), serves as an excellent platform for generating solitons in designed binary grating media. When a sinusoidal AC electric field $E = (0, 0, E\sin(2\pi f t))$ within a frequency f range from 500 Hz to 1 kHz is applied perpendicularly to the nematic slab, solitons can nucleate from programmable patterns. These solitons move perpendicularly to the orientation of homogeneous background, $\hat{n}$. The threshold voltage for soliton generation can be controlled based on the programmed pattern. Regions with lower surface anchoring energy W require less electric energy to generate solitons, thus reducing the threshold voltage in these areas.

To create a homogeneously aligned nematic liquid crystal (NLC) sample with programmable surface anchoring energy, we employ a photoalignment system using a DMD. The fabrication process is schematically illustrated in Fig. 1(a). Initially, we prepare cells with a thickness of $d = 8.0 \pm 0.3$ μm and coat the inner surfaces with a UV-polarization-sensitive sulfonic azo-dye (SD1). To establish a consistent background, the cells are illuminated with linearly polarized UV light at a wavelength of $\lambda = 405$ nm (LEM405C1, JCOPTIX, China), orienting the SD1 molecules perpendicularly to the light's polarization. To reduce the anchoring energy in a specific area, we use an exposure light source with a wavelength of $\lambda = 365$ nm. These areas, generated by the 365 nm light, are superimposed on the orientational background created by the 405 nm light, resulting in regions with weaker anchoring energy. By loading masks onto the DMD, we can manipulate the exposure pattern, controlling the polarization and diameter of the exposure light with a polarizer and an objective [Fig. 1(b)]. Finally, we fill the cells by capillary action of CCN-47, aligning the LC molecules parallel to the SD1.

As depicted in Fig. 1(c), the anchoring energy W within the blue dashed rectangular box is lower than in the surrounding areas, leading to a reduced threshold voltage for soliton generation. At 0 V, the entire structure maintains a homogeneous alignment. As the voltage increases, solitons first appear in the blue dashed rectangular box and eventually fill the entire box once the voltage exceeds the threshold voltage U_{pattern}.

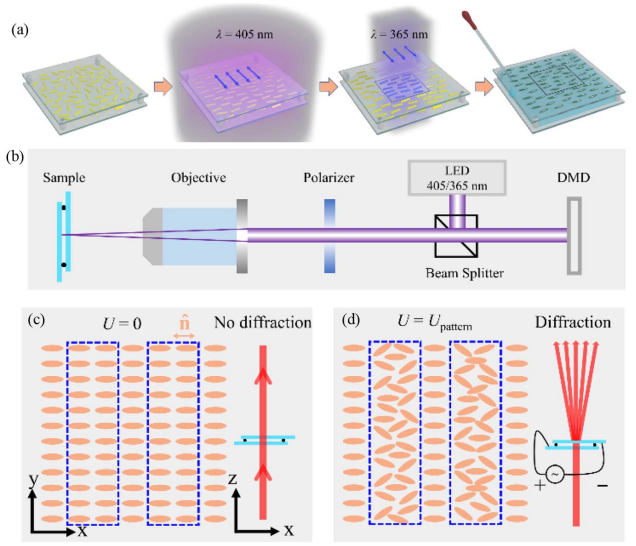

Fig. 1. Schematic of binary grating mediated by solitons for light modulation. (a) Fabrication process of the NLCs sample. Blue arrows represent the linear polarization of UV light. Yellow and light blue short rods depict the SD1 orientation. Green rods denote the optical axis direction of NLCs. (b) Schematic of photoalignment based on a DMD. (c) Distribution of optical axis at $U = 0$ V; laser passes through the sample without diffraction. (d) Distribution of optical axis at $U = U_{\text{pattern}}$; diffraction occurs after laser passes through the sample.

Within the box, the optical axis becomes chaotic, and the azimuthal deviation of $\hat{n}$ from the initial alignment along the x-axis ranges from 20° to 35°. This alternating arrangement of uniform and chaotic states can be regarded as a binary grating, suitable for diffraction devices [Fig. 1(d)].

B. Generation and Localization of Solitons within Reconfigurable Pattern

We created a homogeneously aligned NLC sample using mask 1 and analyzed the kinetics of solitons within a square domain with a side length of $D_1 = 345$ μm [Fig. 2(a)]. The average orientations of the optical axis in the background and the patterned region are denoted as $\hat{n}_1$ and $\hat{n}_2$, respectively [Fig. 2(b)]. Because $\hat{n}_1$ and $\hat{n}_2$ have the same directions, they appear indistinguishable under a polarized optical microscope with crossed polarizers. Thanks to the photolithography process shown in Fig. 1(b), a boundary is created at the intersection of exposed and unexposed areas. When the sample is viewed under a polarizing microscope with crossed polarizers, and both $\hat{n}_1$ and $\hat{n}_2$ are along one of the polarizers, the entire field appears dark due to extinction, making the boundary indistinguishable. By adding an optical compensator ($\lambda = 530$ nm), the local retardance of the nematic changes, and the entire region takes on a dark red hue, allowing the square boundary to become clearly visible [Fig. 2(b)]. The orientation inside and outside the boundary is consistent, but the external anchoring energy is higher than the internal one. If the applied voltage exceeds the threshold for soliton generation, U_{soliton}, solitons can nucleate from irregularities, which are circled in pink [Figs. 2(c) and 2(e)]. The driven force, arising from the coupling between the applied

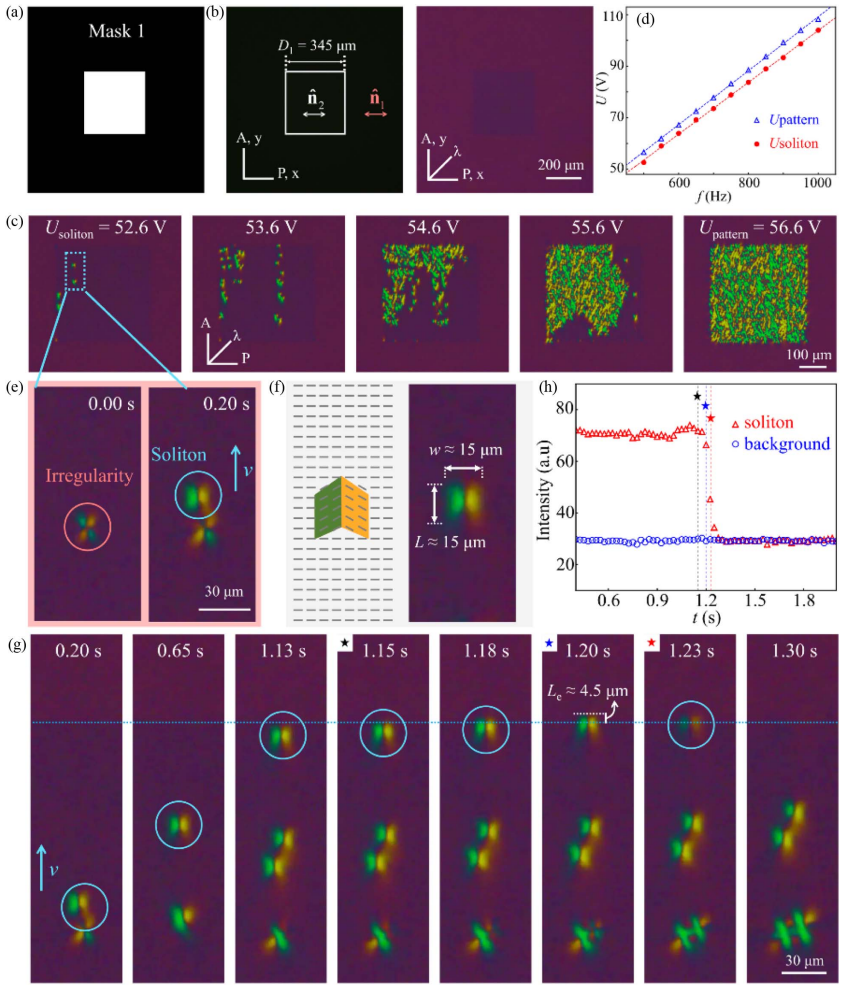

Fig. 2. Localization of solitons within pattern. (a) Mask for single illumination ($\lambda = 365$ nm) to prepare square pattern. (b) Polarized optical micrographs of samples with or without compensator ($\lambda = 530$ nm). Schematic of photoalignment based on a DMD. (c) Polarized optical micrographs of sample when voltage increases from 52.6 to 56.6 V at 500 Hz. (d) Electric conditions corresponding to the states of soliton generation and soliton filling up. (e) Generation of soliton from irregularity. (f) Structure of single soliton. (g) Solitons disappear at the boundary between two domains exposed by light with different wavelengths. Light blue dashed line in (g) indicates the boundary. (h) Comparison on dependence of transmission intensity within soliton and background on time.

electric field and the splay/bend deformation around these irregularities, overcomes the viscous drag to stabilize the solitonic structure [10]. As shown in Fig. 2(c), we can observe yellow and green besides dark red. The reason is that a soliton has two wings and the directors within those two regions are different. When an optical compensator is inserted with the optic axis λ making 45° with the polarizer, one shoulder of the soliton appears yellow and the other blue.

The solitons lack fore-aft symmetry and move perpendicularly to the director ($\hat{n}_2$) [Fig. 2(e)]. The in-plane director deformation within the soliton resembles a bow, resulting in flexopolarization, $P = e_1\hat{n}\nabla\cdot\hat{n} - e_3\hat{n}\times\nabla\times\hat{n}$, where e_1 and e_3 represent the flexoelectric coefficients. This flexopolarization leads to spatial charge density and a corresponding Coulomb force. The flexoelectric force, directed along the soliton movement, helps maintain the stable morphology of solitons. Extensive experimental observations indicate that the soliton width is governed by the sample thickness d, rather than by the mask structure. During motion, solitons maintain a consistent width along the x-axis, approximately $w \approx 2d$. Additionally, the soliton length and width are nearly equal, both measuring approximately 15 μm [Fig. 2(f)]. Once the voltage exceeds another threshold, $U_{pattern}$, solitons expand to fill the entire square with weaker anchoring energy [Figs. 2(c) and 2(d)]. Figure 2(d) provides insights into the electric conditions across diverse frequencies. The red line signifies the threshold for generating solitons within the pattern, $U_{soliton}$, while the blue line corresponds to the threshold for the chaotic phase, $U_{pattern}$.

Solitons are capable of propagating over distances several tens of times their characteristic length and maintaining their integrity following collisions [10]. They are generated continuously and disappear when they reach the boundary [Figs. 2(g) and 2(h)]. When a soliton travels a certain distance beyond the boundary ($L_e = 4.5$ μm), the transmitted light intensity inside the soliton gradually matches the background, indicating that

the soliton gradually disappears [Fig. 2(h)]. This phenomenon likely occurs because stronger anchoring energy requires more electric energy to couple with the flexoelectric effect. The driven force must overcome the viscous drag force to maintain the solitonic structure, leading to soliton emission. Therefore, solitons are first generated within the boundary and disappear at the boundary if the applied voltage is insufficient to initiate soliton emission outside the boundary. Here, we have demonstrated that patterns with weaker anchoring energy are filled with solitons, while the surrounding environment maintains uniform alignment without director perturbation.

C. Optical Diffraction for Binary Gratings Mediated by Solitons

In this work, we applied three additional masks to manipulate areas with lower anchoring energy, aiming to further investigate the potential application for soliton localization (Figs. 3 and 5). Masks 2 and 3 contain six and ten stripes, respectively [Figs. 3(a) and 3(d)]. After an exposure process with a 10 × objective, we measure the stripe widths for masks 2 and 3 as $D_2 = 75$ μm and $D_4 = 56$ μm. These stripes and uniform regions form periodic structures, with single periods of $D_3 = 214$ μm and $D_5 = 136$ μm. By rotating the analyzer counterclockwise by either 20° or −20°, the boundary becomes more apparent in the optical micrographs [Figs. 3(c) and 3(f)]. We then demonstrate binary gratings mediated by solitons and show the diffraction pattern in both experiment and simulation.

As expected, we can confine solitons within periodic patterns irradiated by light at a wavelength of 365 nm (Fig. 4). Using a He–Ne laser directed normally along the z-axis, we captured the resulting diffraction pattern with a camera.

These patterns, comprising numerous solitons, cause the azimuthal deviation of the director from the x-axis to range from 20° to 35°. Different diffraction patterns can be observed under various electric conditions.

Initially, without an applied electric field, no diffraction pattern is observed, and the output image shows a single dot [Fig. 4(a)]. With a constant frequency of $f = 500$ Hz, varied voltages, U, yield different observable phenomena. When the applied voltage, $U = 54$ V, is insufficient to fill the entire region with solitons, we cannot observe obvious diffraction patterns [Figs. 4(b) and 4(c)]. As the voltage increases to $U = 57$ V, the number of solitons increases rapidly, and solitons occupy regions characterized by lower anchoring energy. The substantial number of solitons in a localized region results in an apparent aggregation, giving the impression that they are adhered together. Then, the alternating arrangement of uniform and chaotic states can operate as a grating and result in an obvious 1D diffraction pattern [Figs. 4(d) and 4(e)]. Further increase of voltage leads to the disappearance of the 1D diffraction pattern since the chaos in the low anchoring energy region extends to the entire sample [Fig. 4(f)].

For binary amplitude gratings, multiple slit diffractions under Fraunhofer conditions yield the intensity of the diffracted wave as [36]

$$I = I_0\left(\frac{\sin\alpha}{\alpha}\right)^2\left(\frac{\sin\frac{N\delta}{2}}{\frac{\delta}{2}}\right)^2, \tag{1}$$

where I_0, N, and δ denote the incident light intensity, number of slits, and optical path of the laser. Here, $\alpha = \frac{kxb}{2r}$, where k, x, b, and r represent the wave number, x-coordinate in the diffraction plane, width of the slit, and distance between the sample and diffraction plane, respectively. Additionally, the intensity of the main maximum for binary amplitude gratings is given by [36]

$$I = N^2 I_0\left(\frac{\sin\alpha}{\alpha}\right)^2, \tag{2}$$

indicating that the intensity of the main maximum is proportional to N^2. As mentioned above, the main maximum intensity in the diffraction plane of the ten-period grating is greater than that of the six-period grating [Figs. 4(d) and 4(e)].

To further investigate diffraction in two-dimensional binary gratings, we use mask 4 to fabricate the NLC sample [Figs. 5(a) and 5(b)]. By expanding to two-dimensional gratings mediated by solitons, we can still observe diffraction, as shown in

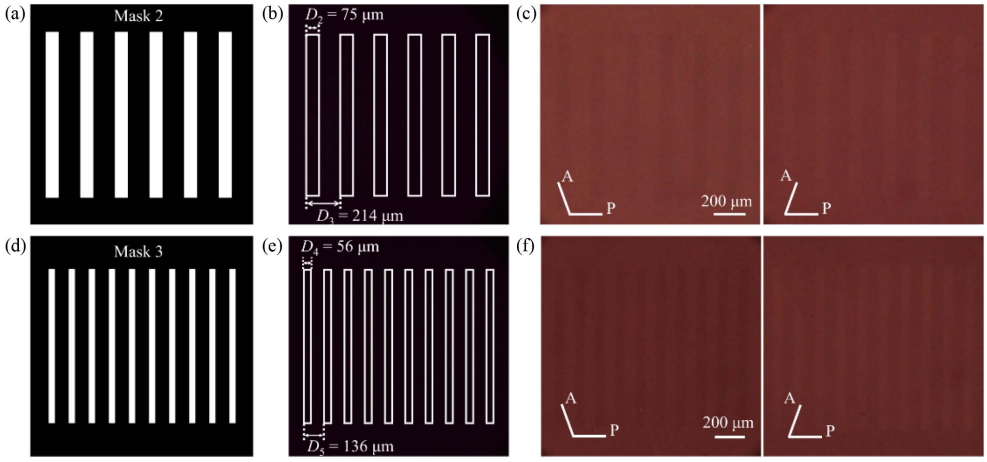

Fig. 3. One-dimensional orientational order system. (a), (d) Masks for single illumination ($\lambda = 365$ nm) to prepare patterns. (b), (e) Optical micrographs of samples under crossed polarizers. Anchoring energy within the rectangle is weaker compared to the surroundings. (c), (f) To distinguish boundaries between patterns more clearly, rotate the analyzer counterclockwise by 20° or −20°.

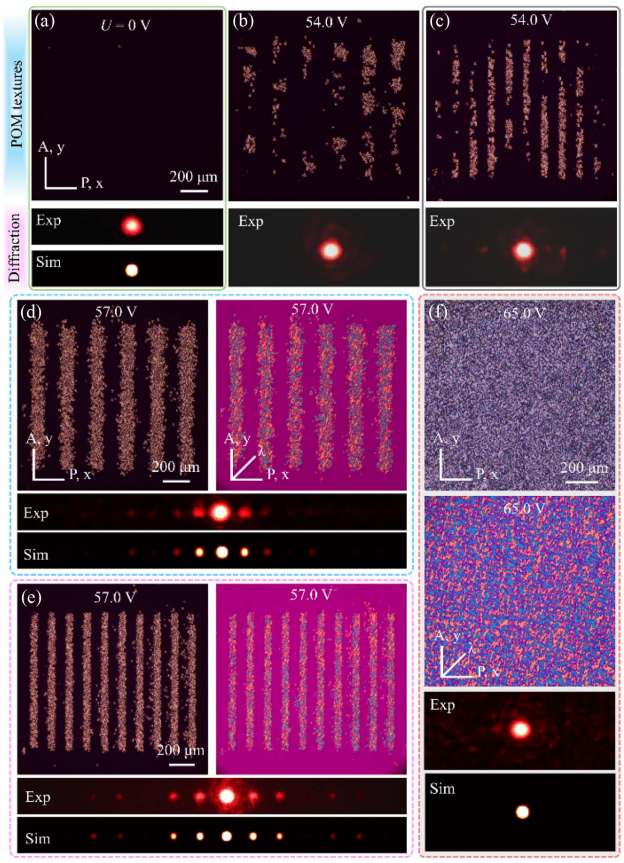

Fig. 4. Optical diffraction for binary gratings mediated by solitons. (a) Uniform state without diffraction. (b), (c) Solitons nucleate from patterns but do not fill patterns. (d) Binary grating with six periods. (e) Binary grating with ten periods. (f) Chaotic phase and corresponding diffraction pattern.

Fig. 5(e). In Figs. 4(b) and 4(c), the solitons do not fully occupy the entire designed pattern, leading to a cloud-like diffraction pattern that tends to expand into 2D. This phenomenon inspired us to design a 2D grating pattern to achieve a clearer 2D diffraction pattern, as shown in Fig. 5. Using mask 4, we fabricate the NLC sample with stripe and single period widths of $D_6 = 66$ μm and $D_7 = 165$ μm [Figs. 5(a) and 5(b)]. When the voltage is 54.5 V, a cloud-like diffraction pattern appears, similar to those in Figs. 4(b) and 4(c). When the voltage is 57 V, the designed grating structures are filled with solitons, resulting in a clear 2D diffraction pattern, as shown in Fig. 5(e). The different diffraction patterns observed under various electric conditions suggest the potential for establishing a system that outputs different information by tuning the electric conditions. This phenomenon indicates promising applications in the field of information science.

3. CONCLUSIONS

In summary, we propose a binary amplitude grating based on three-dimensional director solitons. By photo-patterning homogeneous nematics with a periodic anchoring energy distribution, solitons can form within regions of weaker anchoring energy when an external electric field is applied perpendicularly to the cell. We realize the localization of solitons since the solitons disappear when they reach the boundary. The alternating arrangement of uniform background and soliton-mediated patterns can operate as a binary amplitude grating. By controlling the applied voltage, we can switch the function of devices mediated by solitons. When the electric field is off, a uniform alignment LC cell can be used as a waveplate and the retardance is given by $\frac{2\pi}{\lambda}\Delta nd$. Birefringence Δn is related to temperature; for CCN47, $\Delta n = 0.024$ at 55°C [16]. λ and d are the wavelength of incident light and sample thickness, respectively. We can manipulate the retardance by varying the experimental temperature and d according to actual needs.

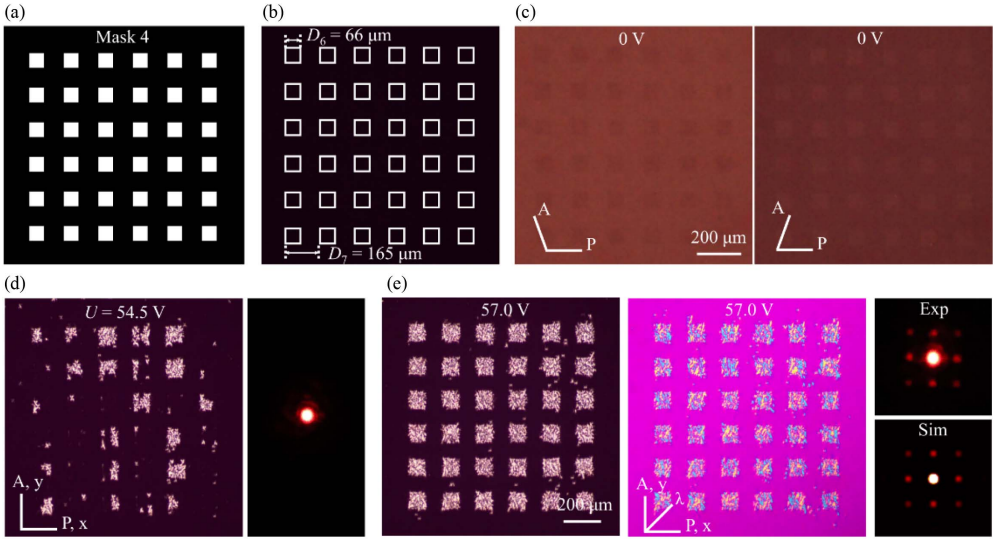

Fig. 5. Two-dimensional binary grating mediated by solitons. (a) Masks for single illumination ($\lambda = 365$ nm) to prepare two-dimensional patterns. (b) Optical micrographs of grating under crossed polarizers. (c) To distinguish boundaries between patterns more clearly, rotate the analyzer counterclockwise by 20° or −20°. (d) Solitons nucleate from patterns but do not fill patterns. (e) Two-dimensional grating. $f = 500$ Hz.

If the suitable voltage is applied across the sample, the cell can act as a diffraction grating. The shape and period of a grating are adjustable, since the weaker anchoring regions can be manipulated by photo-patterning with different masks. This work demonstrates that solitary waves can function as binary amplitude gratings with a response time (∼25 ms) comparable to that of conventional liquid crystal SLMs. Owing to their low fabrication cost and simple design, soliton-based gratings offer a scalable and cost-effective alternative, and more importantly, they extend the practical applications of director solitons beyond micro-cargo transport into optics and information processing technologies.

Funding. National Key Research and Development Program of China (2022YFA1405000); National Natural Science Foundation of China (62375141, 62405147); Natural Science Foundation of Jiangsu Province (BK20243067).

Acknowledgment. Y. L. and B. L. acknowledge the support from Ministry of Science and Technology of the People's Republic of China and Jiangsu Provincial Department of Science and Technology. B. L. and X. T. acknowledge the support from National Natural Science Foundation of China.

Disclosures. The authors declare no conflicts of interest.

Data Availability. Data underlying the results presented in this paper are not publicly available at this time but may be obtained from the authors upon reasonable request.

REFERENCES

1. N. J. Zabusky and M. D. Kruskal, "Interaction of "solitons" in a collisionless plasma and the recurrence of initial states," Phys. Rev. Lett. **15**, 240–243 (1965).
2. T. Dauxois and M. Peyrard, *Physics of Solitons* (Cambridge University, 2006).
3. G. Yel, H. M. Baskonus, and W. Gao, "New dark-bright soliton in the shallow water wave model," Aims Math. **5**, 4027–4044 (2020).
4. M. Bilal, U. Younas, and J. Ren, "Propagation of diverse solitary wave structures to the dynamical soliton model in mathematical physics," Opt. Quantum Electron. **53**, 522 (2021).
5. B. Lautrup, R. Appali, A. Jackson, *et al.*, "The stability of solitons in biomembranes and nerves," Eur. Phys. J. E **34**, 57 (2011).
6. A. Ankiewicz and N. Akhmediev, *Dissipative Solitons: From Optics to Biology and Medicine* (Springer, 2008).
7. Z. Chen, M. Segev, and D. N. Christodoulides, "Optical spatial solitons: historical overview and recent advances," Rep. Prog. Phys. **75**, 086401 (2012).
8. G. Poy, A. J. Hess, A. J. Seracuse, *et al.*, "Interaction and co-assembly of optical and topological solitons," Nat. Photonics **16**, 454–461 (2022).
9. M. Helal and M. Mehanna, "Tsunamis from nature to physics," Chaos Solitons Fractals **36**, 787–796 (2008).
10. B.-X. Li, V. Borshch, R.-L. Xiao, *et al.*, "Electrically driven three-dimensional solitary waves as director bullets in nematic liquid crystals," Nat. Commun. **9**, 2912 (2018).
11. O. D. Lavrentovich, "Design of nematic liquid crystals to control microscale dynamics," Liq. Cryst. Rev. **8**, 59–129 (2020).
12. S. Das, S. Roh, N. Atzin, *et al.*, "Programming solitons in liquid crystals using surface chemistry," Langmuir **38**, 3575–3584 (2022).
13. J.-Z. Lin, A.-J. Wu, L.-T. Zhu, *et al.*, "Fission of quasi-static dissipative solitons in chiral nematics," Giant **19**, 100312 (2024).
14. B.-X. Li, R.-L. Xiao, S. V. Shiyanovskii, *et al.*, "Soliton-induced liquid crystal enabled electrophoresis," Phys. Rev. Res. **2**, 013178 (2020).
15. K.-H. Wu, L.-T. Zhu, F.-F. Xiao, *et al.*, "Light-regulated soliton dynamics in liquid crystals," Nat. Commun. **15**, 7217 (2024).
16. C.-Y. Li, X.-Z. Tang, X. Yu, *et al.*, "Command of three-dimensional solitary waves via photopatterning," Proc. Natl. Acad. Sci. USA **121**, e2405168121 (2024).
17. N. Atzin, A. Mozaffari, X. Tang, *et al.*, "Minimal model of solitons in nematic liquid crystals," Phys. Rev. Lett. **131**, 188101 (2023).
18. B.-X. Li, R.-L. Xiao, S. Paladugu, *et al.*, "Three-dimensional solitary waves with electrically tunable direction of propagation in nematics," Nat. Commun. **10**, 3749 (2019).
19. S. Aya and F. Araoka, "Kinetics of motile solitons in nematic liquid crystals," Nat. Commun. **11**, 3248 (2020).
20. S. Das, N. Atzin, X. Tang, *et al.*, "Jetting and droplet formation driven by interfacial electrohydrodynamic effects mediated by solitons in liquid crystals," Phys. Rev. Lett. **131**, 098101 (2023).
21. Y. Shen and I. Dierking, "Dynamics of electrically driven solitons in nematic and cholesteric liquid crystals," Commun. Phys. **3**, 14 (2020).
22. K.-H. Wu, C.-Q. Chen, Y. Shen, *et al.*, "Trajectory engineering of directrons in liquid crystals via photoalignment," Soft Matter **19**, 4483–4490 (2023).
23. Y. J. Liu, X. Ding, S. C. S. Lin, *et al.*, "Surface acoustic wave driven light shutters using polymer-dispersed liquid crystals," Adv. Mater. **23**, 1656–1659 (2011).
24. G. Si, E. S. Leong, X. Jiang, *et al.*, "All-optical, polarization-insensitive light tuning properties in silver nanorod arrays covered with photoresponsive liquid crystals," Phys. Chem. Chem. Phys. **17**, 13223–13227 (2015).
25. Y. J. Liu, Q. Hao, J. S. Smalley, *et al.*, "A frequency-addressed plasmonic switch based on dual-frequency liquid crystals," Appl. Phys. Lett. **97**, 091101 (2010).
26. L. Wang, H. Dong, Y. Li, *et al.*, "Reversible near-infrared light directed reflection in a self-organized helical superstructure loaded with upconversion nanoparticles," J. Am. Chem. Soc. **136**, 4480–4483 (2014).
27. X. Zhang, Y. Xu, C. Valenzuela, *et al.*, "Liquid crystal-templated chiral nanomaterials: from chiral plasmonics to circularly polarized luminescence," Light Sci. Appl. **11**, 223 (2022).
28. K. Panajotov and M. Tlidi, "Liquid crystal resonator as a nonlinear reflector for passive *Q*-switching and mode locking," Opt. Commun. **549**, 129872 (2023).
29. V. K. Gupta and N. L. Abbott, "Design of surfaces for patterned alignment of liquid crystals on planar and curved substrates," Science **276**, 1533–1536 (1997).
30. V. P. Tondiglia, L. V. Natarajan, R. L. Sutherland, *et al.*, "Holographic formation of electro-optical polymer–liquid crystal photonic crystals," Adv. Mater. **14**, 187–191 (2002).
31. W. Hu, A. Srivastava, F. Xu, *et al.*, "Liquid crystal gratings based on alternate TN and PA photoalignment," Opt. Express **20**, 5384–5391 (2012).
32. J. Kim, J.-H. Na, and S.-D. Lee, "Fully continuous liquid crystal diffraction grating with alternating semi-circular alignment by imprinting," Opt. Express **20**, 3034–3042 (2012).
33. Y. Sasaki, M. Ueda, K. V. Le, *et al.*, "Polymer-stabilized micropixelated liquid crystals with tunable optical properties fabricated by double templating," Adv. Mater. **29**, 1703054 (2017).
34. Z.-G. Zheng, Y. Li, H. K. Bisoyi, *et al.*, "Three-dimensional control of the helical axis of a chiral nematic liquid crystal by light," Nature **531**, 352–356 (2016).
35. R. S. Zola, H. K. Bisoyi, H. Wang, *et al.*, "Dynamic control of light direction enabled by stimuli-responsive liquid crystal gratings," Adv. Mater. **31**, 1806172 (2019).
36. M. Born and E. Wolf, *Principles of Optics: Electromagnetic Theory of Propagation, Interference and Diffraction of Light* (Elsevier, 2013).